Orienting Fatigue Cracks Using Contact Acoustic Nonlinearity in Scattered Plate Waves

Kai WANG,[1‡] Zheng FAN,[2] and Zhongqing SU[1,a)]

[1]*Department of Mechanical Engineering*
The Hong Kong Polytechnic University, Kowloon, Hong Kong SAR

[2] *School of Mechanical and Aerospace Engineering*
Nanyang Technological University, Singapore 639798, Singapore

Submitted to *Smart Materials and Structures*

(Initial submission on 9 May 2018; Revised and re-submitted on 27 June 2018)

‡ PhD student
a) To whom correspondence should be addressed. Tel.: +852-2766-7818, Fax: +852-2365-4703; Email: Zhongqing.Su@polyu.edu.hk (Prof. Zhongqing SU, *Ph.D.*)

Abstract: Targeting quantitative delineation of nonlinear scatterers in elastic media and undersized fatigue cracks in particular, the present study is dedicated to investigation, from analytical, numerical, and experimental perspectives, of the underlying mechanism of interaction between guided ultrasonic waves (GUWs) and "breathing" fatigue cracks – a representative nonlinear scatterer type. Under the modulation of probing GUWs, a "breathing" crack scatters GUWs, in which the crack-triggered contact acoustic nonlinearity (CAN) is embodied. Analytical modeling demonstrates that the extracted CAN manifests unique scattering patterns associated with the crack slant, on which basis the crack can be oriented, without requiring reference to baseline signals. Experimental validation corroborates analytical prediction, in which an embryonic fatigue crack in an aluminum plate waveguide is oriented accurately and visualized in a pixelated image.

***Keywords*:** crack orientation; nonlinear scatterer; contact acoustic nonlinearity; "breathing" fatigue crack

Prevailing material characterization and damage identification methods using nonlinear elastic waves [1-6] rest on a premise that the material plasticity or degradation due to nonlinear scatterers (*e.g.*, fatigue cracks) buried in a waveguide can, to a certain degree, distort guided elastic waves. As a consequence, the nonlinearity embodied in the guided elastic waves is locally intensified in the vicinity of the nonlinear scatterers, on top of the intrinsic material nonlinearity that distributes uniformly in the medium. Among various modalities of nonlinearity, the high-order harmonics in guided elastic waves exhibit high sensitivity to the presence of nonlinear scatterers and therefore have gained prominence for identifying early material degradation and embryonic damage [7-10]. Ordinarily, material-related high-order harmonics manifest in a cumulative manner as wave propagation, provided that probing waves are excited at frequencies at which internal resonance (phase velocity matching and non-zero power flux from the primary to high-order harmonics) takes

place [11, 12]. In contrast, high-order harmonics induced by a nonlinear scatterer in the medium, such as a fatigue crack, are highly restricted within the vicinity of the nonlinear scatterer only. In this case, the nonlinear scatterer-induced high-order harmonics are independent of wave propagation distance and usually overwhelming over other types of nonlinearity including intrinsic material nonlinearity [13]. Exploiting such a phenomenon, approaches for detecting the presence of nonlinear scatterers are legion, albeit to a qualitative degree.

Nevertheless, it is often a vast challenge for these approaches to evaluate the scatterer quantitatively at a more sophisticated level, such as the orientation or severity of an undersized fatigue crack. Although the growth of a fatigue crack demonstrates a complicated, zigzag-like trend at a microscopic level, there is a principal direction along which the crack propagates macroscopically in the order of millimeter. Accurate ascertainment of such a principal direction provides a critical basis for residual life prediction and structural design optimization, whose significance cannot be overemphasized [14]. Knowledge of the crack orientation-related wave scattering phenomena can be beneficial to quantitative evaluation of crack severity which represents a crucial yet unsolved problem in engineering practice. However, there is an obvious lack of demonstrated approaches able to quantitatively evaluate such a principal direction of undersized fatigue cracks, and this can be partially attributed to the shortage of proven theoretical foundation and analytical models that link the nonlinearity of guided elastic waves to a particular damage parameter of interest (*e.g.*, orientation) in a quantitative manner.

To break such a bottleneck of a wave nonlinearity-driven philosophy for the quantitative evaluation of nonlinear scatterers, the contact acoustic nonlinearity (CAN) [15-

17] embodied in guided ultrasonic waves (GUWs) that is induced by a nonlinear scatterer (*e.g.*, a fatigue crack) is here scrutinized analytically, numerically, and experimentally, whereby the scatterer, particularly its orientation, can be delineated. In experimental validation, an embryonic fatigue crack in an aluminum plate waveguide is oriented accurately on the basis of analytical modeling, and the crack is further visualized in a pixelated image by virtue of a diagnostic imaging algorithm.

In the interest of damage evaluation, in what follows we limit the nonlinear scatterer to a hairline fatigue crack in a plate waveguide, in which GUWs take the modality of Lamb waves. The fundamental symmetric Lamb mode (S_0), as the incident probing waves, are selected to interact with the crack. A typical fatigue crack features two free contacting surfaces, the illuminated-side and shaded-side surfaces, as defined in figure 1.

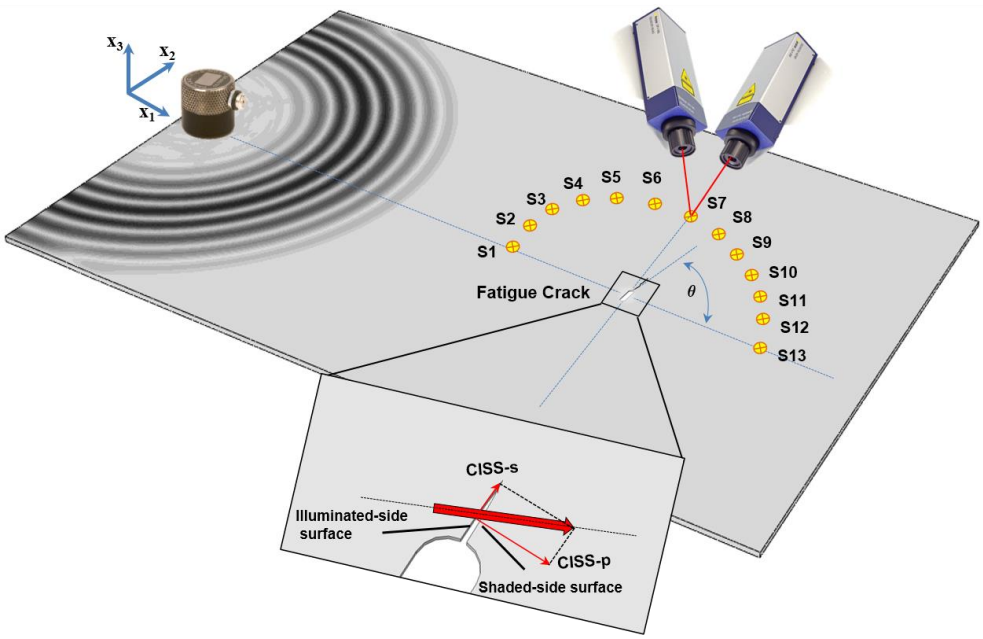

Figure 1. An aluminum waveguide bearing a fatigue crack with an angle of θ regarding wave propagating direction; a transducer is used to excite probing GUWs and a laser vibrometer system measures displacement fields

When the probing GUW traverses the crack, the mutual interaction embraces two coherent half cycles: (i) crack opening during the tensile phase of the probing GUW, inducing wave scattering and mode conversion; and (ii) crack closing during the compressional phase of the probing GUW, without distorting wave propagation. These two half-cycles jointly give rise to "breathing" behavior of the crack that in turn modulates the original GUW and engenders a second wave source to excite additional wave fields in the waveguide. Such a secondary wave source is called a *crack-induced second source* (CISS) in this study. CISS is present when the crack opens and absent otherwise, and that time-dependency leads to the generation of CAN in the additional wave fields.

First consider the stress-free state of the two crack surfaces when the "breathing" crack opens, the CISS on the two crack surfaces can be deemed as additional forces introduced to induce additional wave fields, which offset the probing waves-induced forces on the crack surfaces so that the stress-free condition at the surfaces can be retained. Therefore, the CISS can be defined using the equilibrant forces for the stress fields on the two crack surfaces that are introduced by the probing GUW. Note that the scale of the crack under discussion can be ignored when compared with the distance between the crack and the location at which the GUW is later captured, and thus the CISS on each crack surface can be equivalent to a point force, the magnitude of which is defined by integrating the CISS-induced stress field over each crack surface, as

$$\vec{CISS}^{open} = \int_{Crack\ Surface} -\sigma_0^{inc} \times \vec{x}_1 ds. \tag{1}$$

In the above, σ_0^{inc} signifies the stress tensor of the probing GUW and $\vec{x}_1$ is a vector normal to the crack surface. $\vec{CISS}^{open}$ denotes CISS when the crack opens. CISS is a vector that is

represented by ***CISS*** hereinafter.

Strictly speaking, the spatial displacement of each discretized point on the crack surface is different from the others on the same surface at any moment. However, owing to the minute scale of the crack (less than 1/16 of the wavelength of the probing GUW, to be detailed in subsequent discussion), the discrepancy in the spatial displacement of individual points on a crack surface is negligible. It is a corollary that the moment when the probing GUW changes from the compression into the tension phase is adopted as the moment at which the entire crack, as a whole, commences to open (denoted t_{open}); and in a similar vein, the moment when the probing GUW changes from the tension into the compression phase is the moment for the entire crack to close (denoted t_{close}).

To reflect this cyclic "breathing" behavior, an indicator function, $f(t)$, is introduced to modulate $\overrightarrow{CISS}^{open}$, which reads

$$\overrightarrow{CISS}^{bre} = \overrightarrow{CISS}^{open} \times \mathrm{e}^{i\omega_0 t} \times f(t), \tag{2}$$

where

$$f(t) = \begin{cases} 1, & t_{open} < t < t_{close} \\ 0, & t_{close} < t < t_{open} + T, \end{cases} \tag{3}$$
$$t_{close} = t_{open} + T/2.$$

In Eq. (2), $\overrightarrow{CISS}^{bre}$ is the modulated ***CISS*** with a periodic property, ω_0 the angular frequency of the probing GUW, and T the duration of a cycle of the probing GUW. With Eqs. (2) and (3), each high-order GUW component generated by $\overrightarrow{CISS}^{bre}$ can be defined, including the second-order harmonics at $2\omega_0$. Thus, with the known amplitude of the

second-order harmonic wave modes (denoted $A_{2\omega_0}$), $\overset{\rightarrow}{CISS}^{bre}$ at $2\omega_0$ can be obtained as

$$\overset{\rightarrow}{CISS}^{bre-2\omega_0} = A_{2\omega_0} \times \overset{\rightarrow}{CISS}^{open} \times e^{i2\omega_0 t}. \tag{4}$$

An elasto-dynamic method [18] is recalled to delineate the ***CISS***-induced second-order harmonic wave fields, with $\overset{\rightarrow}{CISS}^{bre-2\omega_0}$ obtained using Eq. (4). The interaction shifts part of the energy carried by the probing GUW to high-order wave modes.

Without loss of generality, if we consider a scenario in which the principal orientation of the crack is NOT tangential to the wavefront of the probing GUW, the $\overset{\rightarrow}{CISS}^{bre-2\omega_0}$ on the crack surfaces can be decomposed into two components, namely (i) *CISS-p* that is normal to the crack orientation and (ii) *CISS-s* that is parallel to the crack orientation, as illustrated schematically in figure 1. Note that the ***CISS***, a vector, has opposite vector directions at the illuminated-side and shaded-side surfaces, see figure 2. The Lamb wave modes induced by *CISS-s* on both surfaces feature identical amplitude yet opposite phase, and they are mutually cancelled in the superposed wave field; on the other hand, the Lamb wave modes generated by *CISS-p* on either crack surface propagate independently and are manifested in a captured GUW signal. Meanwhile, the *CISS-p* on the crack surfaces induces the particulate displacement at the crack tips which is mainly along the crack orientation as a result of the symmetry of the *CISS-p* and the Poisson effect, leading to generation of Lamb wave modes. However, these generated wave modes, compared with Lamb wave modes generated by the stresses on the surfaces, are negligible – as demonstrated in both simulation and experiment.

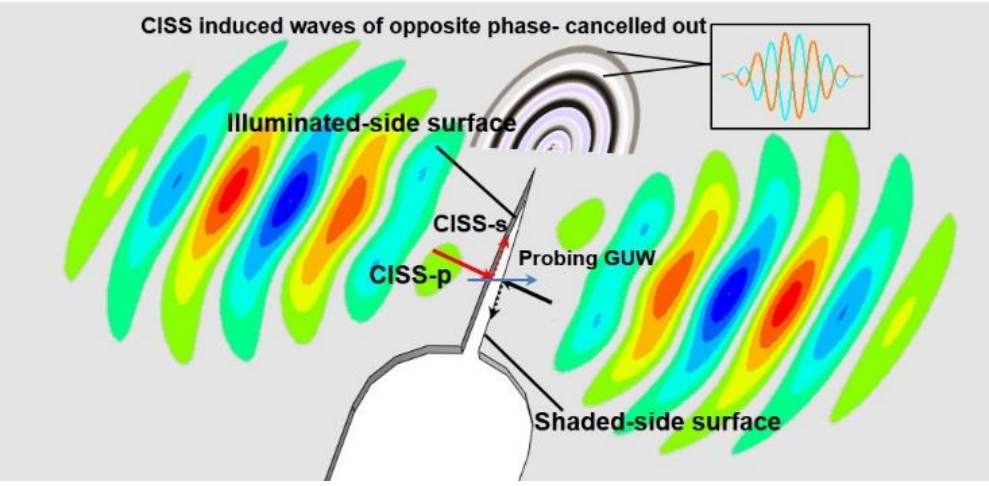

Figure 2. Schematic illustration of interaction between the probing GUW and a "breathing" crack: two components of the ***CISS*** (*i.e.* CISS-s and CISS-p) are generated

With the elasto-dynamic method[18], the displacement of S_0 in the direction of $\vec{x}_1$ induced by $\vec{CISS}^{bre-2\omega_0}$ can be analytically predicted as

$$
\begin{aligned}
{}_{2\omega_0}u_{x_1}^{S_0} = A^{S_0}U^{S_0}\left(x_3\right)\left[H_0^2\left(k_{S_0}r\right) - 1\big/\left(k_{S_0}r\right)\times H_1^2\left(k_{S_0}r\right)\right] \\
\times\cos\left(\theta_1 - \left(\pi/2+\theta\right)\right)\cos\left(\theta_1\right),
\end{aligned}
\tag{5a}
$$

$$
A^{S_0} = \frac{k_{S_0}}{2i}\left[CISS_{in}^{bre-2\omega_0}U^{S_0}\left(x_3\right)\sin\left(\theta\right)\right]\big/I_{S_0S_0}, \tag{5b}
$$

where ${}_{2\omega_0}u_{x_1}^{S_0}$ represents the displacement fields of the S_0 mode at $2\omega_0$ in the $\vec{x}_1$ direction, i the imaginary unit, and θ the angle between wave propagation direction ($\vec{x}_1$) and crack orientation. θ_1 signifies the angle between the path linking the sensing point and the crack and wave propagation direction ($\vec{x}_1$). $CISS_{in}^{bre-2\omega_0}$ is the in-plane component of $\vec{CISS}^{bre-2\omega_0}$. k_{S_0} is the wavenumber of the S_0 mode at $2\omega_0$, and r the distance from the crack to location at which GUW is to be received. $U^{S_0}\left(x_3\right)$ denotes the shape function of the in-plane displacement of the S_0 mode at $2\omega_0$, and H the Hankel function. $I_{S_0S_0}$ is the power

carried by the S_0 mode.

As reflected by Eq. (5a), the wave field of S_0 mode induced by the $\overrightarrow{CISS}^{bre-2\omega_0}$ can be defined analytically and explicitly. It can be observed from Eq. (5) that scattering patterns of crack-induced wave fields are generated at $2\omega_0$, mathematically unique and depending on the crack orientation (*i.e.*, θ). By exploiting these unique wave scattering patterns, the crack orientation (θ) can be ascertained inversely – the underlying premise of this proposed crack orienting approach.

To validate the above analytical model and orient a hairline fatigue crack using the "breathing" effect-induced CAN based on Eq. (5), both finite element (FE) simulation and experiment are implemented. An aluminum plate waveguide (elastic modulus 71.8GPa, density 2660 kg/m^3, Poisson's ratio 0.33), 2 mm in thickness, 500 mm in length, and 300 mm in width, is considered. In simulation using ABAQUS®/EXPLICIT, Hanning-window modulated 5-cycle sinusoidal tone bursts at a central frequency of 300 kHz are excited by applying a pair of symmetric forces on two selected FE nodes on the waveguide free edge that are symmetrically positioned on the upper and lower surfaces of the waveguide, as seen in figure 1. The size of the meshed elements is 0.1 mm – lower than 1/40 of wavelength of the probing wave at excitation frequency (*i.e.*, 1/20 of wavelength of the accordingly generated second-order harmonic wave), which demonstrably suffices to guarantee the accuracy and precision of the numerical simulation. The selection of 300 kHz as the frequency to excite the probing GUW lies in the fact that at 300 kHz the excited probing GUW does NOT satisfy the prerequisites of internal resonance[12], and therefore the amplitude of the material-induced second harmonic embodied in the captured GUW signals is bounded and oscillating. Provided that the position of wave acquisition is prudently

determined to meet the criterion that the distance from the wave source to the crack and then from the crack to the place of wave acquisition equals the dispersion length[12], the material-induced nonlinearity in the captured GUW signals becomes insignificant and consequently the CAN-related nonlinearity induced by the crack is dominant. As an additional merit, the use of GUWs at 300 kHz – a relatively low frequency for GUW excitation – can avoid possible adverse effects of multimodal, dispersive, and dissipative traits at higher frequencies[7].

To model a "breathing" crack in the waveguide, a through-thickness seam crack, 1 mm long and located at the center of the waveguide (figure 1), is defined, and a contact-pair interaction between the illuminated-side and shaded-side surfaces is applied. The slant angle (θ) between the principal orientation of the crack and the propagation direction ($\overset{1}{x}_1$) is set at 75° – a value arbitrarily selected. Time-series GUW signals (wavefront signals) are extracted from 13 FE points (serving as 13 sensing points) located along the periphery of a semi-circle centered at the crack (30 mm from the crack center) and 15° apart, as seen in figure 1. These sensing points are numbered in sequence as *S1*, *S2*, …, *S13*. By application of short-time Fourier transform (STFT)-based signal processing, the amplitude of the second-order harmonic wave mode ($_{2\omega_0}u_{x_1}^{S_0}$ as defined by Eq. (5)) can be ascertained from the spectra of captured GUW wave signals.

The same waveguide (Aluminum 6061-T6) is prepared in the experiment. A through-thickness slot is treated at the center of the waveguide using a fine drilling process, to serve as a crack precursor, from the tip of which a fine fatigue crack is produced under cyclic loads. The slot, 5 mm in length – less than one-third of the wavelength of the GUW excited at 300 kHz – is small enough to warrant a negligible influence on the propagation of GUW in the

waveguide. Upon 120,000 cycles of a cyclic load (5~26 kN; ratio 0.19) applied to the waveguide at a frequency of 10 Hz via a fatigue test machine (GoPoint®, SDF2000), the waveguide is observed to bear a 1 mm hairline fatigue crack from the tip of the crack precursor. A modular nonlinear ultrasonic system (RITEC® RAM-5000 SNAP system) is used to produce an excitation signal that is identical to that used in the simulation. After filtering out the second harmonics that are inevitably included in the signals due to the system, the excitation signal is applied on a transducer (Olympus®, V1548) mounted at the left end of the waveguide surface. Allowing for the fact that the magnitude of a crack-induced CAN is considerably lower than that of the fundamental wave mode, the resolution of the adopted measurement equipment should be sufficiently high in order to assure that CAN can be extracted appropriately and accurately. To this end, a laser vibrometer system (Polytec®, OFV 5000) is employed to capture GUW signals from 13 sensing points at a sampling rate of 50 MHz by measuring the in-plane particulate displacement in the x_1 direction. The system is able to measure the particulate displacement at the order of picometer (10^{-12} m) that is demonstrably sufficient to warrant the desired resolution.

By way of illustration, figure 3 shows the in-plane displacement histories of the signals at $2\omega_0$ acquired from *S3* and *S6*, in which the extracted second harmonic wave modes are highlighted. Compared with the counterpart signals acquired from an intact waveguide beforehand, additional wave packets are contrastively observed. Knowing the time-of-flight of the additional wave packets and the location of the sensing points, the group velocity of each additional wave packet can be ascertained. On this basis, the wave mode of each additional wave packet can be discerned according to its velocity, leading to the conclusion that the additional wave packets are the S_0 mode induced by the crack at $2\omega_0$. From figure 3, the amplitude of the additional wave packet can subsequently be ascertained.

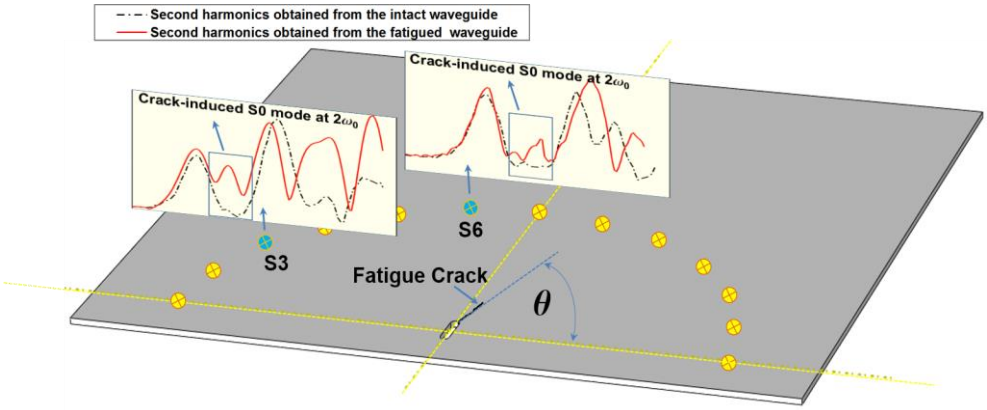

Figure 3. In-plane displacement histories of signals at $2\omega_0$ (compared against counterpart signals from intact waveguide) acquired from *S3* and *S6*

It is noteworthy that this proposed crack orientation method, in principle, does not entail a benchmarking process against the baseline signals from an intact waveguide, because by prudent selection of actuator and sensing point locations, the material-induced second harmonics in the waves are negligible. Therefore, once CAN is identified in the scattered GUW signals, it can confidently be attributed to the presence of fatigue crack, and can be further used to orient the crack based on Eq. (5).

With the amplitude of each crack-induced mode acquired at each inspected point, the wave scattering pattern of the crack-scattered S_0 mode can be obtained. Figure 4 displays the scattering pattern in a polar coordinate system, from which it can be observed that the amplitude of the crack-induced S_0 mode reaches its minimum in the crack orientation direction. The theoretical interpretation into this phenomenon is that the term $\cos\left(\theta_1 - \left(\frac{\pi}{2} + \theta\right)\right)$ in Eq. (5) is zero when $\theta_1 = \theta$, indicating that the minimum of amplitude of the crack-induced S_0 mode is reached in the direction of crack orientation.

Inversely, crack orientation, which is beyond the detection capability of the linear method, can be evaluated using the scattering pattern of the crack-induced S_0 mode at $2\omega_0$. The experimental results corroborate the analytical prediction well.

It is noteworthy that, although the wave scattering pattern is, in theory, dependent on the crack orientation solely and the sensitivity of the proposed method is not restricted by the crack parameters such as orientation or size, there are some practical issues that may negatively affect the detection precision and sensitivity, including mainly the accuracy of measurement equipment, environmental noise, and number of sensing points to name a few. For example, the initial stresses might impose influence on "breathing" behavior of the crack, leading to singularity in crack-induced CAN. With the measurement equipment and techniques adopted in this study, a change of 10 degree in crack orientation, when the crack is 1 mm long, can be characterized precisely and accurately. The nonlinear features of GUWs related to material nonlinearity can be affected by environmental variation (*e.g.* temperature fluctuation) that might also impose influence on the precision and sensitivity of the proposed method. Although a crack might take a complicated modality, there is a principal direction along which the crack propagates, and the proposed method is capable of ascertaining an evaluation for the principal orientation of the crack. When applied to the evaluation of multiple cracks that are densely clustered, waves scattered by the cracks can be mixed, introducing high complexity to a signal and interference in orientation-associated scattering pattern.

Note that generation of CAN does not rely on the wavelength of a probing wave. Different from the approaches making using of linear features of GUW (such as time-of-flight or wave attenuation) in which the wavelength of a probing wave substantially

determines the minimal size of detectable damage, the detectability of the approaches making use of nonlinear features of GUW are, in principle, not restricted by the wavelength of the probing wave.

Ideally, the position of wave acquisition shall be prudently selected, with a hope to minimize the influence of the material nonlinearity, whereby the crack-induced CAN can stand out. In practical implementation, potential crack initiation sites where the stress concentration is prominent can be located using available theory, from which waves can be acquired.

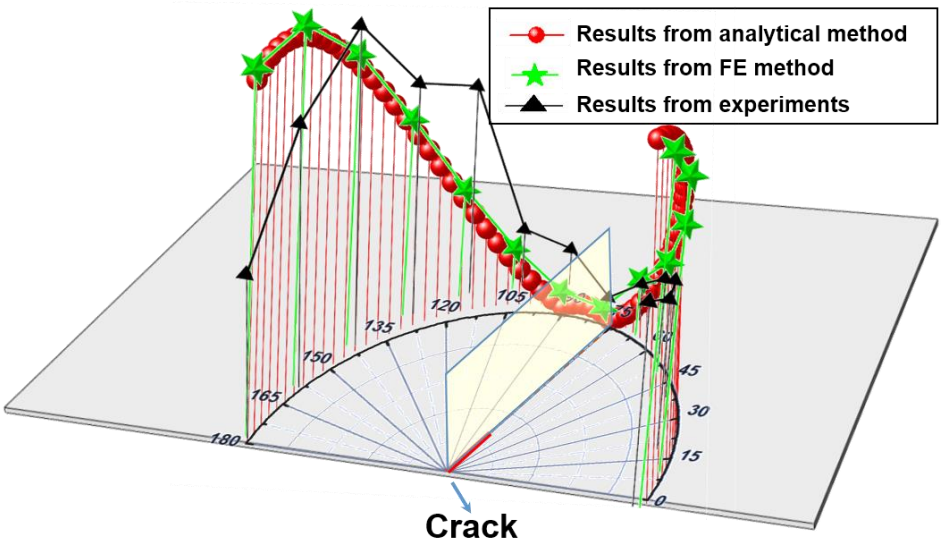

Figure 4. Wave scattering patterns (linked to crack orientation) obtained from analytical, FE, and experimental methods

In this paper, the CAN, generated as a consequence of the interaction between the probing GUW and a nonlinear scatterer (*i.e.*, a fatigue crack). is explored from analytical, simulation, and experimental perspectives. A specific scattering pattern of the CAN embodied in the scattered plate wave fields, depending on the scatterer orientation, is demonstrated. Using CAN, a baseline-free nonlinear scatterer detection technique is

proposed to detect the existence and evaluate the orientation of the nonlinear scatterer. The effective detection of an undersized fatigue crack (less than 1/16 of the probing wavelength) in an aluminum waveguide corroborates the validation of the proposed method. Compared with traditional nonlinear features-based methods, this method can fulfill detection and orientation of the undersized nonlinear scatterer with higher sensitivity, yet without entailing a benchmarking process and beneficial for the deployment of a nonlinear scatterer detection technique using a sparse transducer network.

This work was supported by the Hong Kong Research Grants Council via a General Research Fund (Nos.: 15201416 and 15212417). The authors also acknowledge the support from a Key Project of the National Natural Science Foundation of China (No. 51635008).

[1] C. Zhou, M. Hong, Z. Su, Q. Wang and L. Cheng, Smart Mater. Struct. **22** (1), 015018 (2012).
[2] M. Deng and J. Pei, Appl. Phys. Lett. **90** (12), 121902 (2007).
[3] C. Pruell, J.-Y. Kim, J. Qu and L. J. Jacobs, Appl. Phys. Lett. **91** (23), 231911 (2007).
[4] Z. Parsons and W. Staszewski, Smart Mater. Struct. **15** (4), 1110 (2006).
[5] K. H. Matlack, J.-Y. Kim, L. J. Jacobs and J. Qu, J. Appl. Phys. **109** (1), 014905 (2011).
[6] I. Solodov, J. Wackerl, K. Pfleiderer and G. Busse, Appl. Phys. Lett. **84** (26), 5386-5388 (2004).
[7] C. Bermes, J.-Y. Kim, J. Qu and L. J. Jacobs, Appl. Phys. Lett. **90** (2), 021901 (2007).
[8] P. Fromme, D. E. Chimenti, L. J. Bond and D. O. Thompson, presented at the AIP Conf. Proc., 2014 (unpublished).
[9] A. Klepka, W. Staszewski, R. Jenal, M. Szwedo, J. Iwaniec and T. Uhl, Struct. Health Monit. **11** (2), 197-211 (2012).
[10] J.-Y. Kim, L. J. Jacobs, J. Qu and J. W. Littles, J. Acous. Soc. Am. **120** (3), 1266-1273 (2006).
[11] V. K. Chillara and C. J. Lissenden, Ultrasonics **54** (6), 1553-1558 (2014).
[12] W. De Lima and M. Hamilton, J. Sound Vib. **265** (4), 819-839 (2003).
[13] N. Perez, in *Fracture Mechanics* (Springer, 2017), pp. 187-225.
[14] J. W. Ringsberg, International Journal of fatigue **23** (7), 575-586 (2001).
[15] I. Y. Solodov, N. Krohn and G. Busse, Ultrasonics **40** (1), 621-625 (2002).
[16] J. M. Richardson, Int. J. Eng. Sci. **17** (1), 73-85 (1979).
[17] M. Hong, Z. Su, Y. Lu, H. Sohn and X. Qing, Mech. Syst. Signal Process **60**, 182-197

(2015).
[18] J. Achenbach and Y. Xu, J. Acous. Soc. Am. **106** (1), 83-90 (1999).